The structure of the harmonin/sans complex reveals an unexpected interaction mode of the two Usher syndrome proteins

Jing Yan[1], Lifeng Pan[1], Xiuye Chen, Lin Wu, and Mingjie Zhang[2]

Department of Biochemistry, Molecular Neuroscience Center, Hong Kong University of Science and Technology, Clear Water Bay, Kowloon, Hong Kong

Edited by Jeremy Nathans, Johns Hopkins University, Baltimore, MD, and approved December 29, 2009 (received for review October 3, 2009)

The hereditary hearing-vision loss disease, Usher syndrome I (USH1), is caused by defects in several proteins that can interact with each other in vitro. Defects in USH1 proteins are thought to be responsible for the developmental and functional impairments of sensory cells in the retina and inner ear. Harmonin/USH1C and Sans/USH1G are two of the USH1 proteins that interact with each other. Harmonin also binds to other USH1 proteins such as cadherin 23 (CDH23) and protocadherin 15 (PCDH15). However, the molecular basis governing the harmonin and Sans interaction is largely unknown. Here, we report an unexpected assembly mode between harmonin and Sans. We demonstrate that the N-terminal domain and the first PDZ domain of harmonin are tethered by a small-domain C-terminal to PDZ1 to form a structural and functional supramodule responsible for binding to Sans. We discover that the SAM domain of Sans, specifically, binds to the PDZ domain of harmonin, revealing previously unknown interaction modes for both PDZ and SAM domains. We further show that the synergistic PDZ1/SAM and PDZ1/carboxyl PDZ binding-motif interactions, between harmonin and Sans, lock the two scaffold proteins into a highly stable complex. Mutations in harmonin and Sans found in USH1 patients are shown to destabilize the complex formation of the two proteins.

PDZ | SAM domain | scaffold proteins | USH1C | USH1G

Usher syndrome (USH) is the most common hereditary human disease affecting both the morphology and function of photoreceptor cells in the visual system and hair cells in the auditory system (1–4). USH is clinically and genetically heterogeneous and can be characterized into three forms (USH1, USH2, and USH3). To date, five genes (namely *USH1B*, *USH1C*, *USH1D*, *USH1F.* and *USH1G*) and seven loci are identified for USH1, three genes for USH2 (*USH2A*, *USH2C*, and *USH2D*), and one gene for USH3 (*USH3A*) (1, 4–6). USH1 is the most severe form, characterized by severe congenital deafness, vestibular deficiency, and prepubertal-onset retinitis pigmentosa leading to blindness. In vitro biochemical studies showed that all five USH1 proteins have potential to form large protein complexes (1, 7), although it remains to be established whether such large USH1 complexes exist in vivo. Current data show that the USH1C product, harmonin, is capable of directly binding to all other USH1 proteins (1, 4, 7–10). Consistent with the model that USH1 proteins act in a common molecular pathway, mice containing mutations of any one of the five USH1 proteins share common defects in the stereocilia development of hair cells (11–15). The formation of the USH1 complex is developmental specific. At embryonic stages before formation of stereocilia, harmonin and Sans colocalize with each other at the apical membranes of hair cells where stereocilia will emerge at later stage during development (8). After formation of stereocilia, Sans is restricted to the cuticular plate beneath the apical membrane of hair cells (7), whereas harmonin is concentrated specifically at the upper tip-linker density together with cadherin23 (16). In contrast, the protocadherin15-resident lower tip-linker density is devoid of harmonin (16). It is possible that harmonin binds to a distinct set of proteins during the development of and in the mature hair cells.

Several alternatively spliced transcripts have been reported for USH1C that lead to the generation of various harmonin isoforms. The most prominent of these are harmonin *a*, *b*, and *c* (17). Each isoform contains an N-terminal globular domain (referred to as the N-domain), two PDZ domains, and one or two coiled-coil regions (Fig. 1*A*). Harmonin *a* and *b* each contain an additional PDZ domain at their C termini. Harmonin *b* also contains a Pro, Ser, Th-rich sequence (PST) domain preceding the C-terminal PDZ domain that is known to be responsible for binding to F-actin (8). The N-terminal domain, together with the second PDZ domain of harmonin, binds to the cytoplasmic portion of cadherin23 (8, 9, 18) and anchors the cadherin23 at the upper linker density of hair cell stereocilia (16). It was also reported that the first PDZ domain of harmonin may bind to protein modules, including the globular tail domain of Myosin VIIa and the SAM domain from Sans (7), although such noncanonical PDZ/target interactions are conceptually intriguing.

Sans is another scaffolding protein among the USH1 proteins (10). From N termini to C termini, it contains four ankyrin repeats, a central region, and a SAM domain (Fig. 1*A*). The central region of Sans directly interacts with the tail domain of Myosin VIIa (7), thereby linking harmonin together with the actin-based motor. In Jackson mice containing defective *Sans*, harmonin is completely absent in the hair cells starting at the embryonic stage (11), indicating an obligatory role of Sans in the trafficking of harmonin to stereocilia and implying that the Sans/harmonin interaction contributes to the stability of harmonin.

Here, we report the high resolution complex structure between harmonin and Sans. We discover that the harmonin N-terminal domain and PDZ1 form a structural and functional supramodule that binds to Sans with high affinity. The highly-stable harmonin and Sans complex is formed via synergistic interactions involving a previously uncharacterized PDZ/SAM domain interaction and a canonical PDZ/carboxyl peptide binding. Hearing impairment mutations of harmonin and Sans in USH1 patients are found to disrupt the formation of the harmonin/Sans complex. The structure of the harmonin/Sans complex is expected to be valuable in evaluating the impact of *USH1C* and *USH1G* mutations in future diagnosis of USH1 patients.

Author contributions: J.Y., L.P., X.C., and M.Z. designed research; J.Y., L.P., X.C., and L.W. performed research; J.Y., L.P., and M.Z. analyzed data; and J.Y., L.P., and M.Z. wrote the paper.

The authors declare no conflict of interest.

This article is a PNAS Direct Submission.

Data deposition: The atomic coordinates of the NPDZ1/SAM-PBM complex structure has been deposited in the Protein Data Bank www.pdb.org (PBD ID 3K1R).

[1]J.Y. and L.P. contributed equally to this work.

[2]To whom correspondence should be addressed. E-mail: mzhang@ust.hk.

This article contains supporting information online at www.pnas.org/cgi/content/full/0911385107/DCSupplemental.

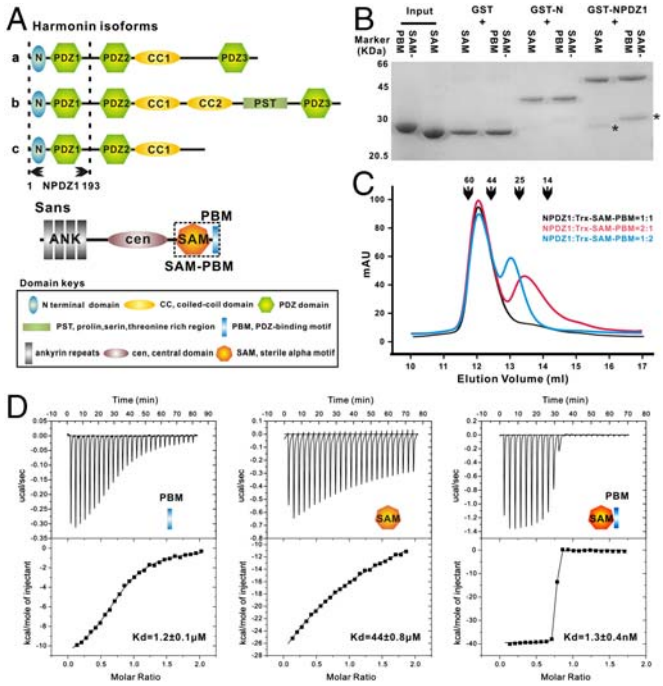

Fig. 1. The multi-dentate interaction between harmonin and Sans. (*A*) A schematic diagram showing the domain organizations of harmonin and Sans. The NPDZ1 and SAM-PBM boundaries used in this study are indicated. (*B*) GST-fusion protein-based pull-down assay showing that NPDZ1 binds to the SAM domain alone and the SAM-PBM of Sans. No interaction between the N-domain and the SAM domain was detected. (*C*) Analytical gel-filtration analysis showing that harmonin NPDZ1 and Sans SAM-PBM forms a 1:1 stoichiometric complex. (*D*) ITC-based measurements of the binding affinities of NPDZ1 with Sans PBM, SAM, and SAM-PBM.

Results and Discussion

The SAM Domain and PBM of Sans Synergistically Bind to the Harmonin NPDZ1 Supramodule. The stable α-helical N-domain of harmonin, together with its second PDZ domain, bind to two separate fragments of the cadherin23 cytoplasmic domain, providing a structural explanation for the stable harmonin/cadherin23 complex found in the tip links of hair cells (11, 16, 18). In this study, we first set out to characterize the structure of the harmonin PDZ1, as the domain has been shown to bind canonical carboxyl peptide ligands (e.g., the C-terminal tails of Sans, Usherin, and VLGR1) as well as the SAM domain of Sans and the tail domain of Myosin VIIa (7, 8, 19). We discovered that the cadherin23-binding N-domain, PDZ1, and a 25-residue extension C-terminus to PDZ1 (residues 1–192, and referred to as NPDZ1) forms an integral structural and functional supramodule (Figs. S1 and S2).

In an earlier study, the interaction between harmonin and Sans was mapped to the NPDZ1 region of harmonin (referred to as "PDZ1" in the study) and the SAM domain containing the C-terminal PBM of Sans (7). The SAM domain is known as a protein–protein interaction module capable of forming homo- or hetero-oligomers (20). The formation of a SAM/PDZ complex is highly unusual given our current understanding of the canonical target-binding modes of both SAM and PDZ domains (20, 21). Therefore, we characterized the interaction between harmonin NPDZ1 and Sans SAM-PBM using purified recombinant proteins. In a pull-down assay, GST-NPDZ1 was found to bind to SAM-PBM robustly (Fig. 1*B*). Deletion of PBM attenuated the interaction, but did not abolish the interaction (Fig. 1*B*), indicating that the SAM domain of Sans directly binds to harmonin NPDZ1 and the NPDZ1/SAM-PBM complex contains two discrete binding sites. Given that the N-domain of harmonin adopts a helix-bundle structure and has a remote conformational similarity to the SAM domain, we tested the potential direct interaction between the N-domain with the Sans SAM domain. No direct interaction involving harmonin N-domain with either Sans SAM domain or SAM-PBM could be detected (Fig. 1*B*), indicating that the harmonin NPDZ1 supramodule is required for binding to the Sans SAM-PBM. By using analytical gel-filtration chromatography, we found that NPDZ1 forms a stable complex with SAM-PBM with a 1:1 stoichiometry (Fig. 1*C*). Next, we dissected the two binding sites by measuring their quantitative binding affinities by isothermal titration calorimetry (ITC), and found that Sans PBM bound to NPDZ1 with a $K_D \sim 1$ μM, and the SAM domain bound to NPDZ1 with a $K_D \sim 40$ μM. Importantly, the K_D for the NPDZ1/SAM-PBM complex was ~1 nM, indicating that the two binding sites act synergistically in the formation of the highly stable harmonin/Sans complex (Fig. 1*D*).

Overall Structure of the NPDZ1/SAM-PBM Complex. To uncover the molecular basis of this unique harmonin/Sans interaction, we sought to determine the crystal structure of the NPDZ1/SAM-PBM complex. The NPDZ1/SAM-PBM complex prepared from the wild type proteins formed large crystals that diffracted to 3.6 Å resolution. We discovered, using NMR-based sample condition screening, that NPDZ1 was prone to charge-mediated nonspecific aggregation (Figs. S1). After numerous trials, we found that substitution of Lys157 with Glu effectively eliminated the nonspecific aggregation of NPDZ1 (*SI Text Results* for a detailed account of the discovery of the K157E-NPDZ1 mutant). The complex prepared by using K157E-NPDZ1 and wild-type SAM-PBM was also crystallized, but the crystals only diffracted to 3.2 Å. We noted that wild-type Sans SAM-PBM tends to form various forms of homo-oligomers in solution (Fig. S3). Among the number of SAM-PBM mutants tested, one with Lys437 substituted with Glu showed mono-dispersed behavior from analytical ultracentrifugation- and NMR-based analysis (Fig. S3). Crystals prepared from the K157E-NPDZ1/K437E-SAM-PBM complex (referred to as the NPDZ1/SAM-PBM complex from here on for simplicity) were diffracted to 2.3 Å resolution. The structure of the complex was solved by the molecular replacement method (Table S1). Each asymmetric unit contains one complex molecule. The NPDZ1/SAM-PBM complex has a 1:1 stoichiometry that is consistent with the biochemical analysis (Fig. 1*C*), and the complex is arch-shaped (Fig. 2). The structure of the complex confirms that the harmonin NPDZ1 forms a structural supramodule with its N-domain and PDZ1 integrated together by a mini-domain formed by the 25-residue extension C-terminal to PDZ1. The structure of the N-domain in the complex is very similar to that of the isolated domain in solution (Fig. S4*A* and *B*).

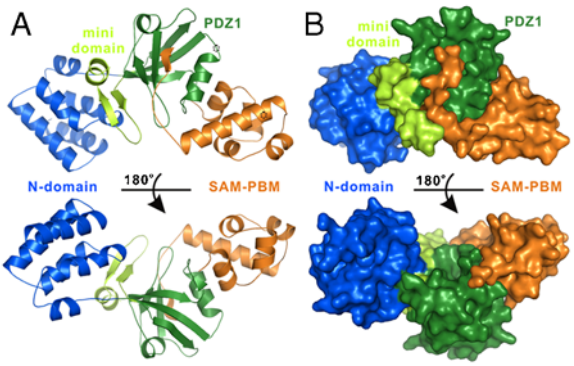

Fig. 2. The overall structure of the NPDZ1/SAM-PBM complex. (*A*) Ribbon diagram of the NPDZ1/SAM-PBM complex structure. In this drawing, the N-domain is shown in *Marine Blue*, PDZ1 domain in *Forest Green*, and mini domain in *Limon Green*. SAM-PBM is drawn in *Orange*. The positions of the two point mutations, K157 in harmonin and K437 in Sans, are indicated with two *Dashed Circles*. (*B*) Surface representation showing the overall architecture of the NPDZ1/SAM-PBM complex with the same color scheme as in panel *A*.

Consistent with the NMR-based analysis (S2*A* and *B*), the solvent exposed hydrophobic cleft formed by the αA/αB-helix hairpin is located at the opposite side of the SAM/PDZ1 interface and fully exposed in the complex (Fig. 2), indicating that the N-domain in the harmonin/Sans complex is still capable of binding to cadherin23. The Sans SAM domain adopts a canonical 5-helix SAM domain fold, and a structural similarity search using the program Dali (22) revealed that it is most similar to the SAM domain of EphA4 (Fig. S4*C* and *D*). The Sans SAM domain packs extensively with the αB and βE of PDZ1, forming a hitherto uncharacterized interaction mode both for SAM and PDZ domains. The C-terminal end of the last α-helix (αE) of Sans SAM is situated at the bottom of the harmonin PDZ1 αB/βB target-binding groove, a geometry that is well suited for Sans PBM to bind to harmonin PDZ1 by augmenting the βB-strand of the PDZ domain (Fig. 2). No direct contact exists between the harmonin N-domain and the Sans SAM-PBM. The two point mutations used to prepare the NPDZ1/SAM-PBM complex are located at the solvent exposed surfaces (indicated with a dashed circles in Fig. 2*A*) and, therefore, are not expected to affect the complex formation.

The NPDZ1 Supramodule of Harmonin. In addition to the N-domain and PDZ1, the amino acid sequences of the linker between the two domains (residues 78–85) and the 25-residue C-terminal extension (residues 168–192) of NPDZ1 are highly conserved (Fig. S5*A*). Parallel with this analysis, these two fragments are found to be exclusively responsible for integrating the N-domain and PDZ1 into a structural and functional supramodule (Fig. 3*A* and *B*). In this NPDZ1 supramodule, the C-terminal extension forms a mini-domain composed of a small β-hairpin followed by an α-helix. The interface between the N-domain and the C-terminal mini-domain is significant (burying ~423 Å^2 surface), considering the small sizes of the two domains. This interface is formed by completely conserved amino acid residues that participate in hydrophobic and charge-charge interactions (Fig. 3*C*). The N-domain and the C-terminal mini-domain are further stabilized by the charge–charge interactions formed between the two positively charge residues in the N-domain PDZ1 linker and two Asp residues from the N-domain (the R80–-D75 and R81–D60 pairs) at the rim of the interface.

The interaction between PDZ1 and the mini-domain extension is primarily mediated by hydrophobic interactions (Fig. S5*A* and Fig. 3*D*). The residues forming the interfaces shown in Fig. 3*C* and *D* are strictly conserved across harmonins from different species (Fig. S5*A*), suggesting that these residues are critical in the assembly of the NPDZ1 supramodule. Mutations of residues in this interface (e.g., K47 and Y184) led to significant weakening of the NPDZ1/SAM-PBM binding even though the sites of the mutations are remote from the interface of the NPDZ1/SAM-PBM, indicating that the structural integrity of NPDZ1 is functionally critical.

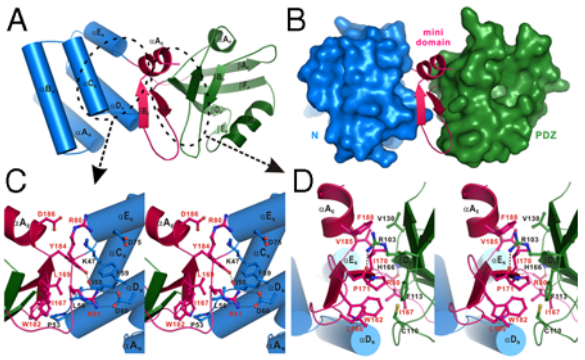

Fig. 3. Assembling of the NPDZ1 supramodule. (*A*) Cartoon diagram showing the NPDZ1 supramodule. In this drawing, the N-domain is shown in *Blue*, PDZ1 domain in *Green*, and the C-terminal mini-domain in *Pinkish Red*. (*B*) Surface representation showing the domain architecture of the NPDZ1 supramodule. (*C* and *D*) Stereo views of the molecular details of the N-domain/mini-domain and PDZ1/mini-domain interfaces, resp. The salt bridges and hydrogen bonds in the interfaces are shown as *Dashed Lines*.

The structure of the NPDZ1 supramodule reveals a unique tandem-domain assembly mode involving PDZ domains. It has been reported that tandem PDZ domains can form supramodules by direct inter-PDZ domain interactions, and such tandem PDZ supramodules include the PDZ12 and PDZ45 tandem from GRIP family proteins, the PDZ12 tandem from X11/Mint family proteins (23), and the PDZ12 tandem from syntenin (24) (Fig. S5*B* and *C*). The structure of NPDZ1 represents a unique example of a PDZ domain that intimately packs with another unrelated protein–protein interaction domain to form a hetero-supramodule. In NPDZ1, the 25-residue extension immediately C-terminal to PDZ1 is vital for the assembly of the supramodule. Would the hetero-supramodule assembly seen in NPDZ1 of harmonin also occur in other PDZ proteins? We analyzed the amino acid sequence features of PDZ domains from the eukaryotic genomes, and found that a substantial amount of PDZ domains contain N- or C-terminal that are highly conserved and predicted to be structured (e.g., the linker between PDZ-GUK tandem in the MAGI family proteins, and the PDZ-SH3 linker in some of the MAGUK family proteins (Fig. S5*D*). It is possible that the hetero-supramodule assembly between a PDZ domain and an unrelated domain, as seen in harmonin NPDZ1, may also exist in other PDZ-containing proteins. Such hetero-supramodule assemblies may explain, at least in part, why a large portion of PDZ domains (~1/3) from the mouse genome could not be properly expressed in bacterial cells (25).

The NPDZ1/SAM-PBM Interface. The Sans SAM-PBM uses both its C-terminal PBM (Fig. 4*A*) and SAM domain (Fig. 4*B*) to form the complex with NPDZ1 that buries a total of ~1, 309 Å^2 surface area. The αB/βB-groove of PDZ1, together with the surface formed between PDZ1 and the C-terminal mini-domain of NPDZ1, forms a continuous Sans-PBM binding surface that accommodates all 8 residues C-terminal to αE of the Sans SAM domain (Fig. 4*A*). The last three residues (T459-L461) of the Sans PBM bind to harmonin PDZ1 via the typical type I PDZ domain/ligand interactions (Fig. 4*A* and *C*). The side chain of D458 from Sans points toward the solvent and forms salt-bridges with R103 and a hydrogen bond with S115 of PDZ1. D458 is evolutionarily conserved in Sans (Fig. S6*A*) and its mutation to Val causes deaf-blindness in humans (26). The side chain of L456 of the Sans PBM inserts into a hydrophobic pocket in NPDZ1 formed by F108, C110, P171, L180, and the aliphatic side chain of K173. In addition to the commonly conserved residues at the 0 and −2 positions for the type I PDZ ligands, all reported harmonin PDZ1 ligands contain an Asp at the −3 position and a hydrophobic residue at the −5 position (Fig. S6*B*), suggesting an extended carboxyl sequence recognition pattern for the PDZ domain.

The interaction between PDZ1 and SAM in the harmonin/Sans complex represents a unique interaction mode for both PDZ and SAM domains. In this interaction, the βE and αB of PDZ1 interacts with αA and αE of SAM, burying a total of ~670 Å^2 surface area (Fig. 4*B* and *D*). Two Arg-Glu pairs of salt bridges ($Arg445_{SAM}$-$Glu148_{PDZ1}$ and $Arg446_{SAM}$-$Glu149_{PDZ1}$) stitch the PDZ1 αB helix and the C-terminal end of SAM αE together. Two hydrogen bonds between the backbone carbonyl of residue $Ser144_{PDZ1}$ and the side chain amide of $R446_{SAM}$, together with the hydrophobic interactions between the side chains of $M450_{SAM}$ and $L106_{PDZ1}$, further strengthen the inter-helix interaction. The entire αA of SAM domain docks onto the surface groove formed by βE and αB of harmonin PDZ1. The hydrophobic interactions between $T394_{SAM}$, $A397_{SAM}$, $C145_{PDZ1}$, and $L153_{PDZ1}$, together with two hydrogen bonds (formed between

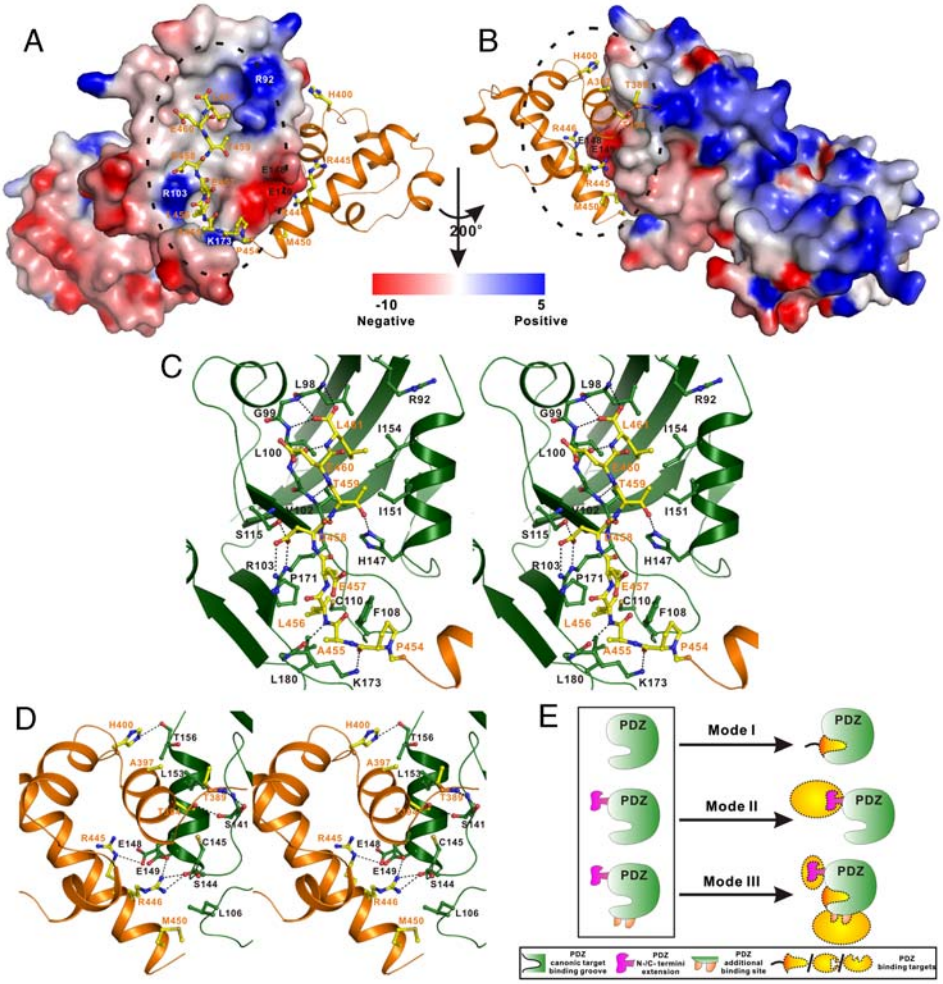

Fig. 4. Molecular details of the harmonin NPDZ1 and Sans SAM-PBM interaction. (*A* and *B*) The combined surface charge representation (NPDZ1) and the stick-ribbon model (SAM-PBM) showing the interaction interface between harmonin NPDZ1 and Sans SAM-PBM. The binding interface between the NPDZ1 and Sans PBM is better viewed in (*A*), whereas the binding interface between the NPDZ1 and Sans SAM is optimally depicted in (*B*). (*C* and *D*) Stereo views showing the detailed interactions between harmonin PDZ1 and Sans PBM (*C*), and between PDZ1 and Sans SAM (*D*). The hydrogen bonds and salt bridges involved in the interfaces are indicated as *Dashed Lines*. (*E*) A schematic cartoon diagram summarizing the three different binding modes of PDZ domains.

the side chain of $T394_{SAM}$ and the backbone carbonyl of $S141_{PDZ1}$ and between the side chains of $H400_{SAM}$ and $T156_{PDZ1}$), mediate the interaction between αA of SAM and βE/αB of PDZ1 (Fig. 4*B* and *D*).

The Sans SAM domain contains two discrete negatively and positively charged surfaces located at the two opposite faces of the domain (Fig. S6*C*), and the domain is likely to form head-to-tail multimers in solution as shown in Fig. S3*A*. The direct interaction between Sans SAM and harmonin PDZ1 prevents the formation of the SAM homo-multimer, as the packing of SAM αA to PDZ1 is mutually exclusive to the packing of SAM αA to αE from the neighboring SAM domain in the SAM dimer model structure (Fig. S6*D*).

The structure of the NPDZ1/SAM-PBM complex reveals a unique mode of PDZ domain-mediated protein interaction. Prior to this study, PDZ-mediated target interactions can be divided into two modes (Fig. 4*E*) (21). Mode I, which is the best characterized, involves the binding of a carboxyl peptide ligand or an internal peptide sequence to the target-binding groove formed by αB and βB of a PDZ domain (Fig. S7*A*). In Mode II, some PDZ domains (e.g., nNOS PDZ and Par-6 PDZ) contain extension sequences either at its immediate N or C termini, and these extension sequences fold together with the PDZ domain and bind to target proteins in a PDZ domain-dependent manner (Fig. S7*B* and *C*). The interaction observed in harmonin PDZ1 can be categorized as a unique (third) binding mode (Fig. 4*E*) that contains features from the first two modes as well as an additional interaction surface (i.e., formed by βE and αB of harmonin PDZ1 domain) for binding to another target protein (the SAM domain in this case). Given the large number of PDZ domain proteins in mammalian genomes (e.g., ∼200 PDZ proteins and ∼300 non-redundant PDZ domains in the human genome), it is likely that other PDZ domains may interact with multiple targets using the unique binding mode that we have discovered for harmonin PDZ1.

Syndromic Mutations Found in Human Patients Destabilize the Harmonin/Sans Complex. We next investigated the interaction between harmonin and Sans and the effect of the missense mutations of harmonin and Sans associated with USH1 on the harmonin/Sans complex formation using HeLa cells as the model system. When expressed individually, harmonin *a* displays a diffused localization both in the cytosol and nucleus, whereas Sans shows a punctuate staining pattern distributed exclusively in the cytoplasm of transfected cells (8, 10). Co-transfection of harmonin *a* and Sans leads to very good co-localization of the two proteins in the cytosol (Fig. 5*D*), consistent with the tight complex formation of the two proteins observed in vitro (Fig. 1). Deletion of the SAM-PBM domain does not substantially change the distribution pattern of Sans, indicating that the N-terminal ankyrin repeats and/or the central region of Sans is largely responsible for the cytoplasmic puncta formation of Sans (Fig. 5*E*). When the full length harmonin *a* is co-expressed with Sans lacking the SAM-PBM domain, harmonin is diffused both in the cytosol and nucleus (Fig. 5*E*), indicating that the SAM-PBM-mediated binding of Sans to harmonin is essential for cellular co-localization of the two proteins. A 20-base pair deletion mutation of *USH1G* found in USH1 patients produces mutant Sans lacking

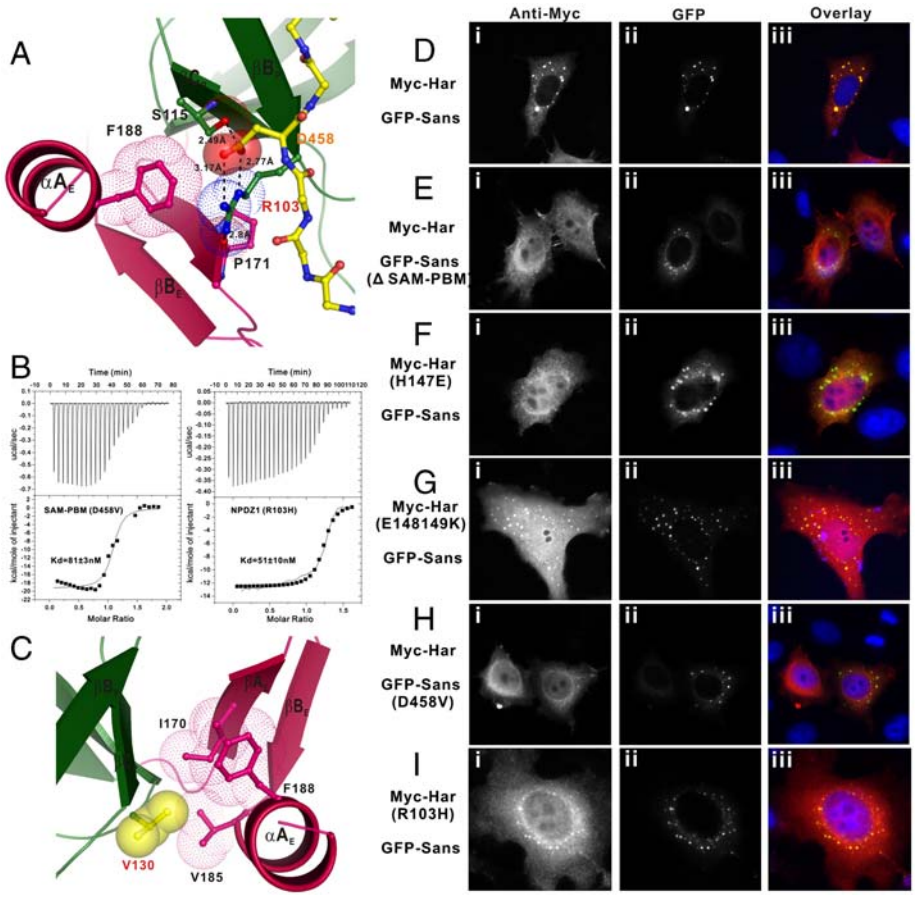

Fig. 5. Syndromic mutations found in human patients destabilize the harmonin/Sans complex. (*A-C*) Detailed structural diagrams showing the three residues (D458 from Sans, R103, and V130 from harmonin) identified in USH patients. (*A*) The combined ribbon and the stick-dot-sphere representations showing the critical roles of Sans D458 and harmonin R103 residues in the harmonin PDZ1/Sans PBM interaction. (*B*) ITC-based measurements of the binding affinities of the NPDZ1/D458-SAM-PBM complex and the R103H-NPDZ1/SAM-PBM complex. (*C*) Enlarged view of the hydrophobic packing environment of harmonin V130, indicating that the substitution of this Val with Ile should not have major impact on the overall structure of the harmonin/Sans complex. (*D–I*) Both the PDZ1/PBM and PDZ1/SAM interactions are critical for the formation of the stable harmonin/Sans complex in HeLa cells. (*D1–D3*) When cotransfected in HeLa cells, harmonin *a* co-localizes with the Sans clusters in cytosol. (*E1–E3*) Deletion of SAM-PBM compromises the co-localization of harmonin *a* and Sans. (*F1–F3*) and (*G1–G3*) Mutations that weaken either the PDZ1/PBM or the PDZ1/SAM interactions attenuate the co-localization of harmonin and Sans. (*H1–H3*) and (*I1–I3*) Two mutants, Sans D458V (*H1–H3*) and harmonin R103H (*I1–I3*), identified in USH1 patients, also attenuate the colocalization of harmonin and Sans.

the entire SAM-PBM (10). Based on the structure of the harmonin/Sans complex solve here, this Sans mutant loses its capacity to interact with harmonin.

We next dissected the roles of the two discrete binding sites observed in the NPDZ1/SAM-PBM complex structure in the cellular co-localization of harmonin *a* and Sans. To assess the role of the harmonin PDZ1/Sans PBM interaction, we constructed a harmonin mutant with H147 at the αB1 position of PDZ1 substituted with Glu, as this substitution is known to abolish the binding of the canonical PBM to the type I PDZ domain (21). When cotransfected, the majority of H147E-harmonin is diffused throughout the cells. However, weak mutant harmonin puncta could be observed, and these harmonin puncta again overlap well with the Sans puncta (Fig. 5*F*), consistent with the in vitro biochemical study that the PDZ1/PBM interaction is critical for the formation of the stable harmonin/Sans complex (Fig. 1). To evaluate the PDZ1/SAM interaction in the harmonin/Sans co-localization, we used a K148,149E-mutant of harmonin, as substitutions of the two Lys residues in the αB-helix of PDZ1 with Glu would specifically weaken or eliminate the PDZ1/SAM interaction (Fig. 4*D*). When co-expressed, K148,149E-harmonin has two distinct populations: one is largely diffused throughout the cells, and the other shows as puncta throughout the cytoplasm that overlap well with the Sans puncta (Fig. 5*G*), suggesting that the PDZ1/SAM interaction is also critical for the cellular co-localization of harmonin and Sans.

We next investigated the cellular localization patterns of a Sans mutant (D458V) and a harmonin mutant (R103H), both of which are known to cause hearing/visual impairments in USH1 patients (26, 27). D458 in Sans plays a critical role for the PDZ1/PBM interaction by forming a pair of salt bridges with R103 and a strong hydrogen bond with S115 of harmonin (Fig. 4*C* and Fig. 5*A*). The D458V mutation disrupts both the salt bridge and the hydrogen bonding interactions seen in the wild-type harmonin/Sans complex, and leads to ∼60-fold decrease in the binding affinity of the harmonin/Sans complex (Fig. 5*B*). Consistent with this structural and biochemical analysis, harmonin is largely diffused throughout the cells when the protein is co-expressed with D458V-Sans (similar to the H147E mutant of harmonin, Fig. 5*H*). The R103H-NPDZ1 binds to Sans SAM-PBM with about ∼40-fold lower affinity than the wild-type NPDZ1 (Fig. 5*B*). The R103H mutation of harmonin is expected to have a somewhat milder effect on PDZ1/PBM binding, as the substituted His partially retains a charge–charge interaction with D458 from Sans PBM (Fig. 4*C* and Fig. 5*A*). Consistent with this structural and biochemical analysis, puncta staining of R103H-harmonin was observed when the mutant protein is co-expressed with Sans (Fig. 5*I*). It is worth noting that the R103H mutant of harmonin is more diffused with some nuclear distributions when compared to the wild-type protein (Fig. 5*D*). A V130I missense mutation occurred in harmonin PDZ1 was found in an USH1 patient (28). Although V130 is directly involved in the hydrophobic packing of PDZ1 with the C-terminal mini-domain, its substitution with an Ile is unlikely to alter the complex assembly as V130 is partially surface-exposed (Fig. 5*C*). Consistent with this structural analysis, the mutation (caused by G388A mutation in *USH1C*) is known to introduce a unique splicing site in the exon 5 of *USH1C*, leading to the truncation of the majority of the protein (28). Taken together, the cellular co-localization study of harmonin and Sans and their respective mutants indicated that the high affinity bidentate NPDZ1/SAM-PBM complex shown in this study is likely to be critical for the stable association of the harmonin/Sans complex in vivo.

In summary, the structure of the harmonin/Sans complex determined in this work provide an atomic picture showing the assembly of the two core components of the USH1 proteins. The harmonin/Sans complex may serve as a platform to interact with many other proteins related to the development of hearing and visual cells in mammals via a number of other unoccupied domains in the complex. The structure of the harmonin/Sans complex also expands our understandings, in general, of the interaction modes for both PDZ and SAM domains. Finally, in addition to providing molecular explanations to the disease-causing mutations already identified in USH1 patients, the structure of the harmonin/Sans complex will be valuable in rationalizing other mutations that might be discovered in these two USH1 scaffold protein in the future.

Materials and Methods

Protein Preparation. The coding sequence of harmonin NPDZ1 (residues 1–192) was PCR amplified from human *USH1C* and cloned into a pET32a vector. Protein was expressed in BL21(DE3) *Escherichia coli* cells. The His_6-tagged N-domain was purified as described earlier (18). For in vitro biochemical analysis, the wild-type NPDZ1 and its mutants were expressed as either His_6-tagged or GST-fused proteins. The recombinant proteins were purified either with Ni^{2+}-nitrilotriacetic acid agarose column or with GSH-Sepharose column, followed by another step of gel-filtration chromatography. The coding sequences of Sans SAM-PBM (residues 384–461) and SAM (384–458) were PCR amplified from human *USH1G* gene.

Crystallography. Crystals of harmonin NPDZ1 in complex with Sans SAM-PBM were obtained by the hanging drop vapor diffusion method at 16 °C. Freshly purified complex protein was concentrated to 15 mg/ml. The NPDZ1/SAM-PBM complex was set up in hanging drops with equal volume of 0.2 M $CaAc_2$, 0.1 M HEPES, pH 7.5, and 18% (w/v) polyethylene glycol 10000. Glycerol (10%) was added as the cryo-protectant. A 2.3 Å resolution X-ray dataset was collected at 100 K by a Rigaku R-AXIS IV++ imaging-plate system with a MicroMax-007 copper rotating-anode generator. The diffraction data were processed using the MOSFLM and scaled by the SCALA modules in the CCP4 suite (29). The complex structure was solved and refined as described in *SI Text Materials and Methods*. The final refinement statistics are listed in Table S1.

Analytical Ultracentrifugation. Sedimentation velocity experiments were performed on a Beckman XL-I analytical ultracentrifuge equipped with an eight-cell rotor at 25 °C. The final sedimentation velocity data were analyzed and fitted to a continuous sedimentation coefficient distribution model with the fitting result shown as solid lines using the program SEDFIT (http://www.analyticalultracentrifugation.com/default.htm).

GST Pull-Down Assay. Direct interactions between harmonin NPDZ1 and various Sans fragments were assayed in phosphate-buffered saline (pH 7.4). Equal molar amounts of GST-NPDZ1 and Sans fragments (~0.6 nmol each) were mixed in 100 μl of the assay buffer. The GST-NPDZ1/Sans complexes were pelleted by adding 15 μl of fresh GSH-Sepharose beads. The pellets were washed three times with 0.5 ml of the assay buffer and, subsequently, detected by using SDS-PAGE.

Isothermal Titration Calorimetry Assay. ITC measurements were carried out on a VP-ITC calorimeter (MicroCal) at 25 °C. All protein samples were in 50 mM, pH 7.5 Tris buffer plus 100 mM NaCl. The titration processes were performed by injecting 10 μl aliquots of the Sans fragments into harmonin NPDZ1 proteins at time intervals of 3 min to ensure that the titration peak returned to the baseline.

Cellular Localization Assay. Wild-type harmonin *a* was cloned into the pCMV-Myc vector, and Sans was cloned into the pEGFP.C3 vector. EGFP-Sans lacking the SAM-PBM (EGFP-Sans ΔSAM-PBM) and different mutants were created using the standard PCR-based method. HeLa cells were transiently transfected with 0.5 μg of each plasmid per well using lipofectamine *PLUS* kit (Invitrogen), and cells were cultured for 24 h before fixation. The cells were imaged with a Nikon Eclipse TE2000 (Nikon) inverted fluorescence microscope.

ACKNOWLEDGMENTS. We thank Miss Ling-Nga Chan for the help in cell biology experiment, Drs. Jiang Yu and Yanxiang Zhao for the help in crystallography, and Dr. Conan Wang for careful reading of the manuscript. This work was supported by grants from the Research Grants Council of Hong Kong to M.Z. (6442/06M, 663407, 663808, 664009, CA07/08.SC01, AoE/B-15/01-II, and SEG_HKUST06). The NMR spectrometers used in this work were purchased with funds donated to the Biotechnology Research Institute by the Hong Kong Jockey Club.

1. Reiners J, Wolfrum U (2006) Molecular analysis of the supramolecular usher protein complex in the retina. Harmonin as the key protein of the Usher syndrome. *Adv Exp Med Biol* 572:349–353.
2. El-Amraoui A, Petit C (2005) Usher I syndrome: Unravelling the mechanisms that underlie the cohesion of the growing hair bundle in inner ear sensory cells. *J Cell Sci* 118:4593–4603.
3. Ahmed ZM, Riazuddin S, Wilcox ER (2003) The molecular genetics of Usher syndrome. *Clin Genet* 63:431–444.
4. Kremer H, van Wijk E, Marker T, Wolfrum U, Roepman R (2006) Usher syndrome: Molecular links of pathogenesis, proteins and pathways. *Hum Mol Genet* 15:R262–270 Spec No 2.
5. Williams DS (2008) Usher syndrome: Animal models, retinal function of Usher proteins, and prospects for gene therapy. *Vision Res* 48:433–441.
6. Ebermann I, et al. (2007) A novel gene for Usher syndrome type 2: Mutations in the long isoform of whirlin are associated with retinitis pigmentosa and sensorineural hearing loss. *Hum Genet* 121:203–211.
7. Adato A, et al. (2005) Interactions in the network of Usher syndrome type 1 proteins. *Hum Mol Genet* 14:347–356.
8. Boeda B, et al. (2002) Myosin VIIa, harmonin and cadherin 23, three Usher I gene products that cooperate to shape the sensory hair cell bundle. *EMBO J* 21:6689–6699.
9. Siemens J, et al. (2002) The Usher syndrome proteins cadherin 23 and harmonin form a complex by means of PDZ-domain interactions. *P Natl Acad Sci USA* 99:14946–14951.
10. Weil D, et al. (2003) Usher syndrome type I G (USH1G) is caused by mutations in the gene encoding SANS, a protein that associates with the USH1C protein, harmonin. *Hum Mol Genet* 12:463–471.
11. Lefevre G, et al. (2008) A core cochlear phenotype in USH1 mouse mutants implicates fibrous links of the hair bundle in its cohesion, orientation and differential growth. *Development* 135:1427–1437.
12. Johnson KR, et al. (2003) Mouse models of USH1C and DFNB18: Phenotypic and molecular analyses of two new spontaneous mutations of the Ush1c gene. *Hum Mol Genet* 12:3075–3086.
13. Self T, et al. (1998) Shaker-1 mutations reveal roles for myosin VIIA in both development and function of cochlear hair cells. *Development* 125:557–566.
14. Di Palma F, et al. (2001) Mutations in Cdh23, encoding a new type of cadherin, cause stereocilia disorganization in waltzer, the mouse model for Usher syndrome type 1D. *Nat Genet* 27:103–107.
15. Alagramam KN, et al. (2001) The mouse Ames waltzer hearing-loss mutant is caused by mutation of Pcdh15, a novel protocadherin gene. *Nat Genet* 27:99–102.
16. Grillet N, et al. (2009) Harmonin mutations cause mechanotransduction defects in cochlear hair cells. *Neuron* 62:375–387.
17. Verpy E, et al. (2000) A defect in harmonin, a PDZ domain-containing protein expressed in the inner ear sensory hair cells, underlies Usher syndrome type 1C. *Nat Genet* 26:51–55.
18. Pan L, Yan J, Wu L, Zhang M (2009) Assembling stable hair cell tip link complex via multidentate interactions between harmonin and cadherin 23. *P Natl Acad Sci USA* 106:5575–5580.
19. Reiners J, et al. (2005) Scaffold protein harmonin (USH1C) provides molecular links between Usher syndrome type 1 and type 2. *Hum Mol Genet* 14:3933–3943.
20. Qiao F, Bowie JU (2005) The many faces of SAM. *Sci STKE* 2005:re7.
21. Zhang M, Wang W (2003) Organization of signaling complexes by PDZ-domain scaffold proteins. *Acc Chem Res* 36:530–538.
22. Holm L, Sander C (1998) Touring protein fold space with Dali/FSSP. *Nucleic Acids Res* 26:316–319.
23. Long JF, et al. (2005) Autoinhibition of X11/Mint scaffold proteins revealed by the closed conformation of the PDZ tandem. *Nat Struct Mol Biol* 12:722–728.
24. Kang BS, et al. (2003) PDZ tandem of human syntenin: Crystal structure and functional properties. *Structure* 11:459–468.
25. Stiffler MA, et al. (2007) PDZ domain binding selectivity is optimized across the mouse proteome. *Science* 317:364–369.
26. Kalay E, et al. (2005) A novel D458V mutation in the SANS PDZ binding motif causes atypical Usher syndrome. *J Mol Med* 83:1025–1032.
27. Roux AF, et al. (2006) Survey of the frequency of USH1 gene mutations in a cohort of Usher patients shows the importance of cadherin 23 and protocadherin 15 genes and establishes a detection rate of above 90%. *J Med Genet* 43:763–768.
28. Blaydon DC, et al. (2003) The contribution of USH1C mutations to syndromic and non-syndromic deafness in the UK. *Clin Genet* 63:303–307.
29. Storoni LC, McCoy AJ, Read RJ (2004) Likelihood-enhanced fast rotation functions. *Acta Crystallogr D* 60:432–438.